

Formulation and assessment of narrow-band vegetation indices from EO-1 Hyperion imagery for discriminating sugarcane disease

Armando Apan¹, Alex Held², Stuart Phinn³, and John Markley⁴

¹Geospatial Information and Remote Sensing Group, Faculty of Engineering and Surveying,
University of Southern Queensland, Toowoomba 4350 QLD Australia
Phone: +61 7 4631 1386, Fax: +61 7 4631 2526, Email: apana@usq.edu.au

²Environmental Remote Sensing Group, CSIRO Land and Water,
PO Box 1666, Canberra ACT 2601 Australia
Phone: +61 2 6246 5718, Fax: +61 2 6246 5800, Email: Alex.Held@csiro.au

³Biophysical Remote Sensing Group, School of Geography, Planning & Architecture,
University of Queensland, Brisbane 4072 Australia
Phone: +61 7 3365 6526, Fax: +61 7 3365 6899, Email: s.phinn@uq.edu.au

⁴Mackay Sugar, Post Office Pleystowe, Pleystowe 4741 QLD Australia
Phone: +61 7 4953 8571, Fax: +61 7 4953 8590, Email: j.markley@mkysugar.com.au

ABSTRACT

The increasing commercial availability of hyperspectral image data promotes growing interests in the development of application-specific narrow-band spectral vegetation indices (SVIs). However, the selection of the optimum SVIs for a particular purpose is not straightforward, due to the wide choice of band combinations and transformations, combined with specific application purposes and conditions. Thus, the aim of this study was to develop an approach for formulating and assessing narrow-band vegetation indices, particularly those from EO-1 Hyperion imagery. The focus of SVI development was for discriminating sugarcane areas affected by 'orange rust' (*Puccinia kuehnii*) disease in Mackay, Queensland, Australia. After a series of pre-processing and post-atmospheric correction techniques, an empirical-statistical approach to SVI development was designed and implemented. This included the following components: a) selection of sample pixels of diseased and non-diseased areas, b) visual examination of spectral plots to identify bands of maximum spectral separability, c) generation of SVIs, d) use of *multiple discriminant function analysis*, and e) result interpretation and validation. From the forty existing and newly developed vegetation indices, the output discriminant function (i.e. a linear combination of three indices) attained a classification accuracy of 96.9% for the hold-out sample pixels. The statistical analyses also produced a list of function coefficients and correlation rankings that indicate the predictive potential of each SVI. The newly formulated '*Disease-Water Stress Indices*' (*DSWI*) produced the highest correlations. The approach designed for this study provided a systematic framework in the formulation and assessment of SVIs for sugarcane disease detection.

KEYWORDS: hyperspectral remote sensing, spectral vegetation indices, sugarcane disease, Hyperion

Introduction

Spectral indices are always the result of a compromise, and different indices must be defined for different purposes. Govaert, et al. (1999: 1856)

Hyperspectral remote sensing increases our ability to accurately map vegetation attributes (Curran, 2001; Kumar, et al., 2001). Images acquired simultaneously in narrow spectral bands may allow the capture of specific plant attributes (e.g. foliar biochemical contents) previously not viable with broadband sensors. For example, the use of narrow spectral bands allowed the development of *photochemical reflectance index* (PRI) that was found correlated with carotenoid/chlorophyll ratios in green leaves (Sims and Gamon, 2002). Moreover, in mapping forests in Canada, hyperspectral data produced better classification accuracy than multispectral data (Goodenough, et al., 2002).

One of the approaches used for extracting and mapping vegetation biophysical variables from remotely sensed data is based on spectral vegetation indices (SVIs). SVIs are dimensionless, radiometric measures that function as indicators of relative abundance and activity of green vegetation (Jensen, 2000). They have long been used in remote sensing (e.g. the *Normalised Difference Vegetation Index* (NDVI) developed by Rouse et al., 1973), and there are now more than 20 indices developed from broadband multispectral imagery. As the availability and use of hyperspectral data is growing, the development and application of vegetation indices is expected to increase further.

Vegetation indices can be formulated using various techniques. At the higher end of complexity, one approach used rigorous procedures called *Facility for the Automatic Creation of Optimal Spectral Indices* (FACOSI), which involved radiative transfer models and optimisation technique (Govaert, et al., 1999). The complexity and data-intensive models involved in this approach have so far limited its adoption. On the relatively less complicated side, the use of empirical–statistical approach is common: spectral data from field or laboratory samples are collected and analysed using statistical techniques (e.g. Carter, 1994).

The aim of this study was to develop an empirical–statistical approach on how to formulate and assess narrow-band vegetation indices, particularly those from EO-1 Hyperion imagery. The focus of SVI development was on discriminating sugarcane areas affected by ‘orange rust’ (*Puccinia kuehnii*) disease in Mackay, Queensland, Australia. While we have already reported some aspects of this study elsewhere (Apan, et al., submitted), this current paper focused more on the SVI derivation methodology.

Spectral vegetation indices

Vegetation indices are often used in mapping vegetation attributes and conditions. Studies have shown that vegetation indices, e.g. NDVI, are related to plant biophysical properties, such as leaf area index, percent green cover, green biomass, and amount of photosynthetically active radiation absorbed by the canopy (e.g. Tucker, 1979; Tucker, et al., 1985; Daughtry, et al., 1992). However, the use of VIs has a key limitation: its values are affected by perturbing factors related to soil background, atmosphere, and nonphotosynthetic components of vegetation (Richardson and Wiegand, 1977; Huete, 1988; Kaufman and Tanre, 1992).

The selection of the optimum SVIs for a particular purpose is not straightforward, due to the wide choice of band combinations and transformations, combined with specific application purposes and conditions. While several vegetation indices are functionally redundant in information content (Perry and Lautenschlager, 1984), some of them perform better for specific vegetation attributes. These improved SVIs focused on reducing the impacts of extraneous factors, such as soil brightness changes (e.g. *Soil Adjusted Vegetation Index* (SAVI)) and atmospheric effects (*Atmospherically Resistant Vegetation Index* (ARVI)) (e.g. Huete, 1988; Kaufman and Tanre, 1992). Others focused on the issue of linearity and saturation problems, e.g. *Transformed Difference Vegetation Index* (TDVI) (Bannari, et al., 2002).

Research methods

Study area

The study area is located near Mackay (149° 4' E and 21° 15' S), Queensland (figure 1). The region is the largest sugar-producing area in Australia. It is dominated by subtropical weather patterns: heavy rainfall in summer and typically dry weather during winter. The area’s topography varies from flat alluvial plains where sugarcane crops predominate, to gently undulating topography in the southern part dominated by native woody vegetation.

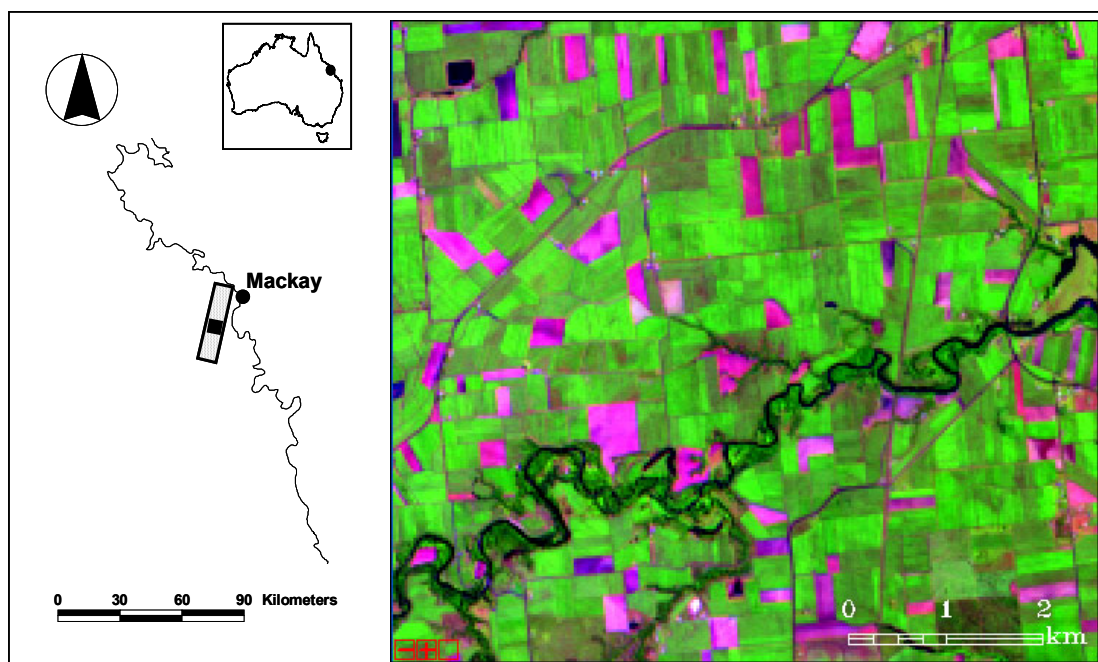


Figure 1 Hyperion image subset (1660, 860, 680nm in RGB) captured over a section of the Mackay sugarcane region on 2 April 2002

A Hyperion image was acquired over the study area on 2 April 2002. It covers 242 bands spanning the wavelength range from 356 nm to 2577 nm, with nominal bandwidths of 10 nm (Pearlman, et al., 2001). Hyperion has two spectrometers: one for the visible and near-infrared (VNIR: 356 nm to 1058nm) region, the other for short-wave infrared (SWIR: 852nm to 2577nm). The sensor, on board the NASA's EO-1 satellite, covers a swath width of 7.6 km with a 30-m ground pixel size.

Hyperion data and preprocessing

The image was delivered as Level 1B_1 data in scaled radiance units (Barry, 2001). To facilitate the development of indices and measurements, these values were converted to apparent surface reflectance using ACORN 4.10 atmospheric correction software (Analytical Imaging and Geophysics LLC, 2002). Prior to this conversion, however, the following preprocessing steps were implemented: *re-calibration*, *band selection*, *de-streaking* and *removal of bad pixels* (figure 2) (Datt, et al., submitted; Apan and Held, 2002).

Re-calibration of the Level 1B_1 data was performed to bring a uniform calibration gain for each band, as well as for better interpretation of radiance spectra. The original 242 bands were then reduced to 176 bands, by excluding the zero data bands, VNIR/SWIR overlap, and the strong water vapour absorption bands. De-streaking, or the removal of non-periodic along-track striping, was implemented using the 'local' destreaking method (Datt, et al., submitted). The removal of bad pixels involved interpolation or complete removal of a line or column (e.g. the first line and the 256th column which contain no data).

A minimum noise fraction (MNF) transformation smoothing was applied to the post-atmospheric correction reflectance image to minimise uncorrelated spatial noise. The technique was applied to the VNIR and SWIR bands separately: only the first 12 VNIR and the first 8 SWIR MNF good bands (i.e. minimum noise) were utilised. This was followed by applying the *Empirical Flat Field Optimal Reflectance Transformation* (EFFORT) polishing technique (Boardman, 1998). The final corrected image was in apparent surface reflectance (multiplied by 10000).

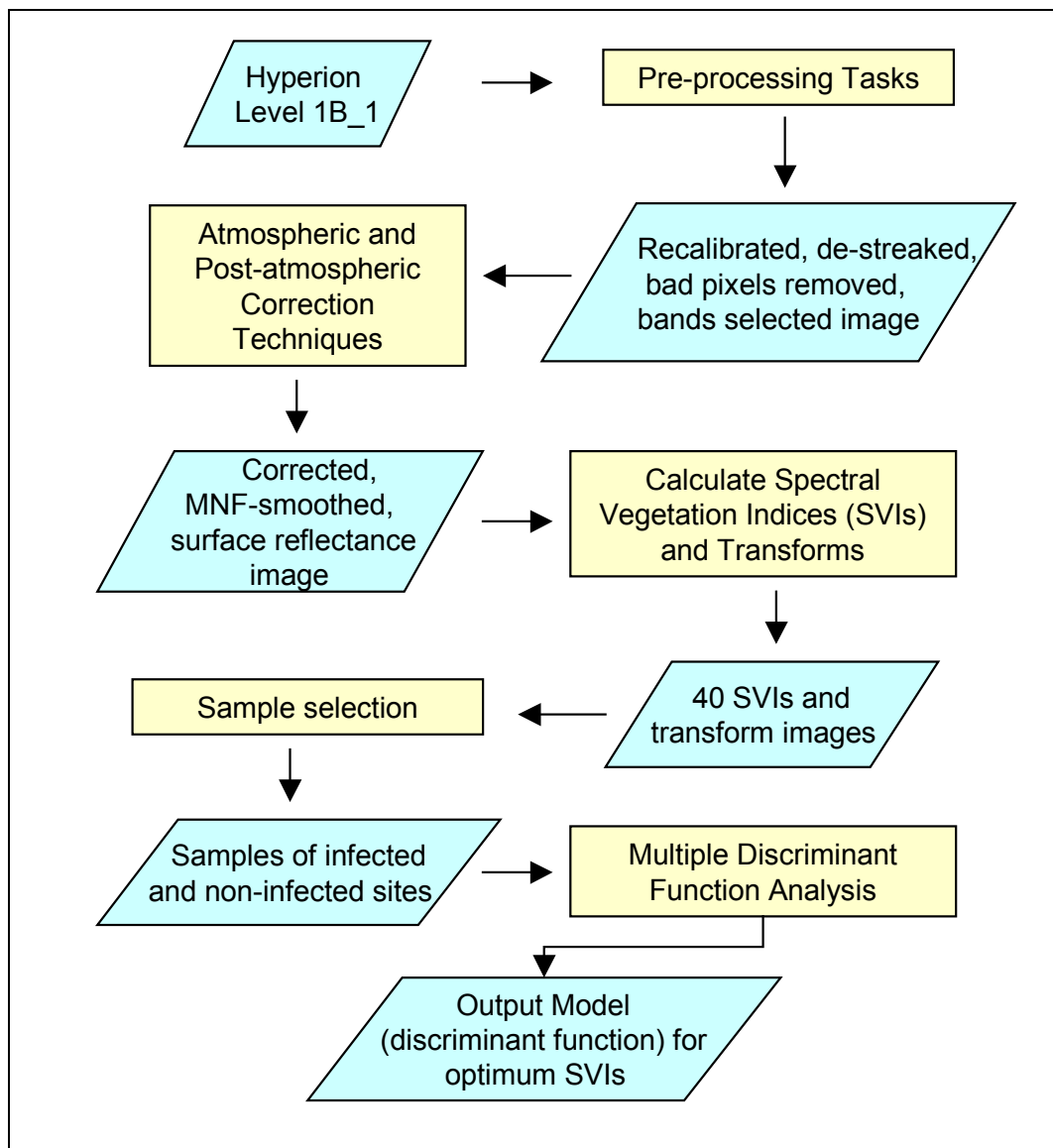


Figure 2 Processing steps in the formulation and assessment of spectral vegetation indices from EO-1 Hyperion for discriminating sugarcane disease

The sugarcane disease

The sugarcane 'orange rust' disease is a fungal disease. It produces leaf lesions (pustules) that are orange in colour and tend to be grouped in patches. The ruptured leaves allow water to escape from the plant, leading to moisture stress (Croft, et al., 2000). Orange rust occurs in summer/autumn and is favoured by humid warm conditions (spore germination optimum at 17–24°C and 97% and above relative humidity). In 1999–2000, the disease caused severe damage to the widely grown variety *Q124*. For the sample pixels in this study, the infection was rated as '4', based on a 1–5 scale (1 has lowest severity to 5 with highest severity).



Figure 3 Leaf symptoms of orange rust (Source: Croft et al., 2000)

Generation of hyperspectral indices

The symptoms of orange rust can be related to changes in leaf pigments, internal leaf structure, and moisture. Thus, spectral vegetation indices (SVIs) that focus on one or more attributes associated with these symptoms were selected (table 1). The majority of which was sourced from the literature, while five new indices were formulated in this study based from the following steps:

- **Collection of sample pixels.** Three sugarcane paddocks affected with the orange rust disease ('disease' class) were digitised from the displayed colour composite, producing a total of 142 sample pixels. Similarly, no-rust areas ('no disease' class), corresponding to the same variety (Q124) and age group as those in the affected plots, were digitised to produce 159 pixels.
- **Visual examination of spectral plots.** Basic statistics (minimum, maximum, mean, and standard deviation) were computed for each class, and then interactively displayed in plots. The difference of the means (i.e. the reflectance values of 'disease' class was subtracted from the 'no disease' class). This step was aimed to determine the spectral bands and/or region with the highest potential for discrimination. Two aspects of spectral plots were considered:
 - *magnitude of difference*—the greater the difference, the greater the potential of band(s) for discrimination;
 - *direction of relationship*—bands or regions that showed inverse relationship was particularly considered, as they were candidates for spectral ratioing technique. For instance, in theory, the red and NIR reflectance have inverse relationship for green vegetation, i.e. red bands have low reflectance values while NIR bands have higher values.
 - *combination of magnitude and direction*—mathematically, two bands with the greatest difference in magnitude and at the same time opposite in direction (i.e. low value in one band vs. high value in another band) will be the best candidate for band ratioing.
- **Formulation of vegetation indices.** Based from graphical plots and statistics, equations were formulated using simple ratios and normalised ratios. In this study, we developed several variants of '*Disease-Water Stress Indices*' (*DSWI*) (formula in Table 1).

Table 1 Vegetation indices used in this study

Name	Formula	References
1. Simple Ratio (SR) 750/705	$R750/R705$	Gitelson & Merzlyak, 1994
2. Simple Ratio (SR) 800/550	$R800/R550$	
3. Normalised Difference (ND) 750/660	$(R750-660)/(R750+R660)$	
4. Normalised Difference (ND) 800/680	$(R800-R680)/(R800+R680)$	Sims & Gamon, 2002
5. Normalised Difference (ND) 750/705	$(R750-R705)/(R750+R705)$	Gitelson & Merzlyak, 1994
6. Modified Simple Ratio (MSR) 705/445	$(R750-R445)/(R705-R445)$	Sims & Gamon, 2002
7. Modified Normalised Difference (MND) 750/705	$(R750-R445)/(R750+R705-2R445)$	Sims & Gamon, 2002
8. Simple Ratio (SR) 750/550	$R750/R550$	Gitelson & Merzlyak, 1994
9. Chlorophyll Well (Chloro-well)		CSIRO VegSpectra (unpublished)
10. Green Peak Well (Green-well)		CSIRO VegSpectra (unpublished)
11. Average reflectance (750 to 850)	Average reflectance between 750 and 850 nm	Strachan, et al., 2002
12. Modified Chlorophyll Absorption in Reflectance Index (MCARI)	$[(R700-R670)-0.2(R700-R550)](R700/R670)$	Daughtry et al., 2000
13. Transformed Chlorophyll Absorption in Reflectance Index (TCARI)	$3[(R700-R670)-0.2(R700-R550)](R700/R670)$	Haboudane, et al., 2002
14. Optimised Soil-Adjusted Vegetation Index (OSAVI)	$(1+0.16)(R800-R670)/(R800+R670+0.16)$	Rondeaux, et al., 1996
15. Ratio TCARI/OSAVI	TCARI/OSAVI	Haboudane, et al., 2002
16. Plant Senescence Reflectance Index (PSRI)	$(R680-R500)/R750$	Merzlyak, et al., 1999
17. Structure-Insensitive Pigment Index (SIPI)	$(R800-R445)/(R800-R680)$	Penuelas, et al., 1995
18. Photochemical Reflectance Index (PRI)	$(R531-R570)/(R531+R570)$	Gamon, et al., 1992
19. Pigment Specific Simple Ratio (Cholophyll a) (PSSRa)	$R800/R680$	Blackburn, 1998
20. Pigment Specific Simple Ratio (Cholophyll b) (PSSRb)	$R800/R635$	Blackburn, 1998
21. Simple Ratio (SR) 695/420	$R695/R420$	Carter, 1994
22. Simple Ratio (SR) 695/760	$R695/R760$	Carter, 1994
23. Red Edge Inflection Point (Lagrangian model) (REIP-Lagr)	(see author)	Dawson & Curran, 1998
24. Red Edge Inflection Point (polynomial model) (REIP-poly)	(see author)	Broge & Leblanc, 2001
25. Principal component 1 (PC1)	principal component transformation	
26. Principal component 2 (PC2)	principal component transformation	
27. Disease-Water Stress Index 1 (DSWI-1)	$R800/R1660$	this study
28. Disease-Water Stress Index 2 (DSWI-2)	$R1660/R550$	this study
29. Disease-Water Stress Index 3 (DSWI-3)	$R1660/R680$	this study
30. Disease-Water Stress Index 4 (DSWI-4)	$R550/R680$	this study
31. Disease-Water Stress Index 5 (DSWI-5)	$(R800+R550)/(R1660+R680)$	this study
32. NDWI-Hyperion (NDWI-Hyp)	$(1070-1200)/(1070+1200)$	Ustin, et al., 2002
33. Normalised Difference Water Index (NDWI)	$(R860-R1240)/(R860+R1240)$	Gao, 1996
34. Water Index (WI)	$R900 / R970$	Penuelas, et al., 1997
35. Ratio of WI and Normalised Difference 750/660	$WI / ND750$	
36. Moisture Stress Index (MSI)	$R1600 / R820$	Hunt & Rock, 1989
37. Water Well 3PT (983) (WW 983)		CSIRO VegSpectra (unpublished)
38. Water Well 3PT (983) (WW 1205)		CSIRO VegSpectra (unpublished)
39. Ratio of WW 983 and PSSRa	$WW\ 983/PSSRa$	
40. Ratio of WW 1205 and PSSRa	$WW\ 1205/PSSRa$	

^a R = reflectance
Source: Apan, et al., submitted.

Statistical analyses

We assessed the performance of vegetation indices using a *multiple discriminant function analysis* (also called canonical discriminant analysis) with a stepwise variable selection method (SPSS, 2001). The procedure generates one or more discriminant functions based on linear combinations of the predictor variables that provide the best discrimination between groups. It has been used successfully in spectral discrimination studies (e.g. Strachan, et al., 2002, Peñeulas, et al., 1994).

The *standardised canonical discriminant function coefficients* provide information on the contribution or 'discriminating ability' of each variable (i.e. SVIs) to the model (SPSS, 2001). On the other hand, the *structure matrix* shows the correlation of each predictor variable with discriminant function. Moreover, to derive and interpret the canonical correlation statistic (R_c) in a way similar with the more common Pearson correlation coefficient (R), a series of single-variable run (i.e. the predictor variable was entered one-at-a-time) was also made to produce R_c for each independent variable. The validation of the model was performed by classifying a 'hold-out sample' (i.e. those pixels not included in model generation) corresponding to 30% of the total sample pixels.

Results and discussion

Visual examination of spectral plots revealed the regions where diseased and non-diseased sample areas can be differentiated (figures 4 to 7). The highest separability based on magnitude is located in the NIR region (approx. between 750 to 880nm and in 1070nm). This was followed by selected ranges in the SWIR region (separability peaked at 1660nm and 2200nm), green (550nm) and red (680nm). Disease-affected areas have relatively lower reflectance values than unaffected sites in the green and NIR regions. However, the reverse is true for the red and the SWIR domains—areas with orange rust have higher reflectance values than no-rust sugarcane.

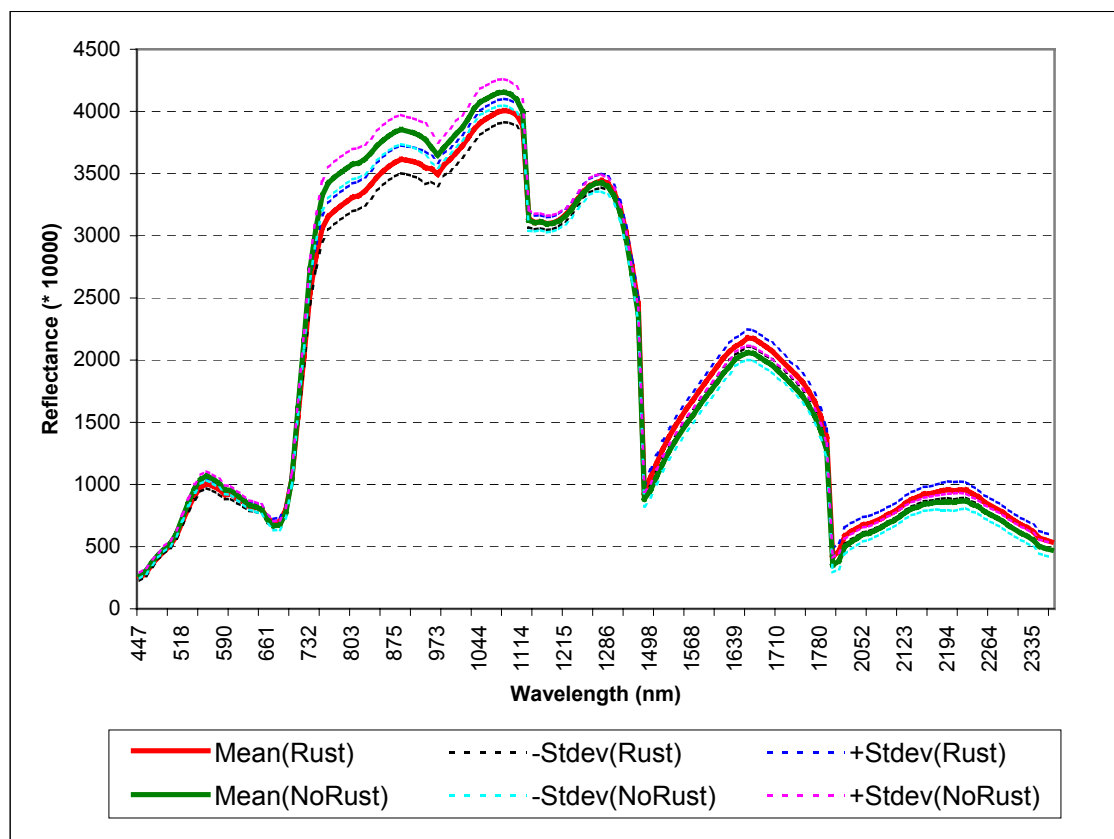


Figure 4 Mean reflectance spectra (447–2365nm) of Hyperion sample pixels containing sugarcane orange rust disease and without orange rust disease

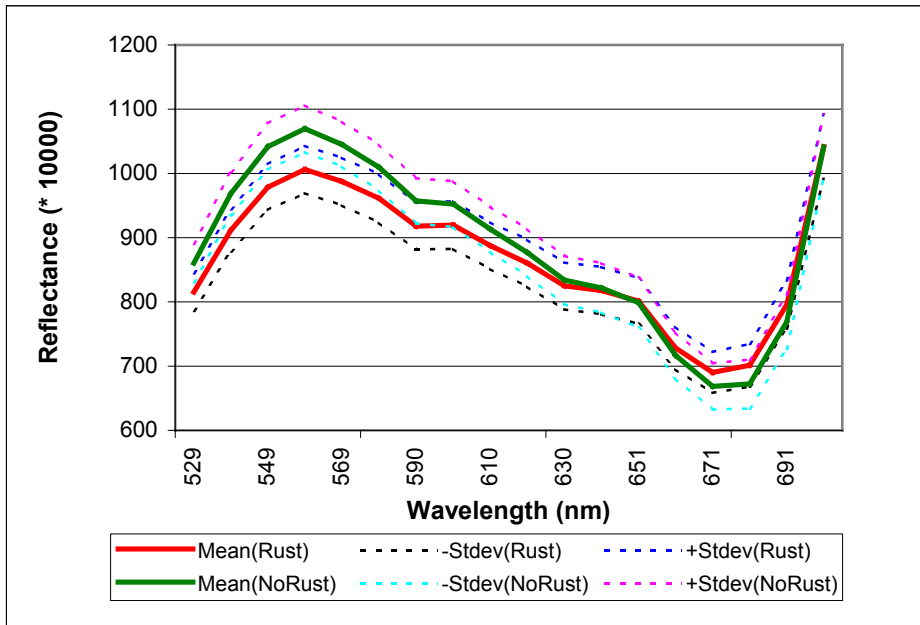


Figure 5 Mean reflectance spectra (528–701nm) of Hyperion sample pixels containing sugarcane orange rust disease and without orange rust disease

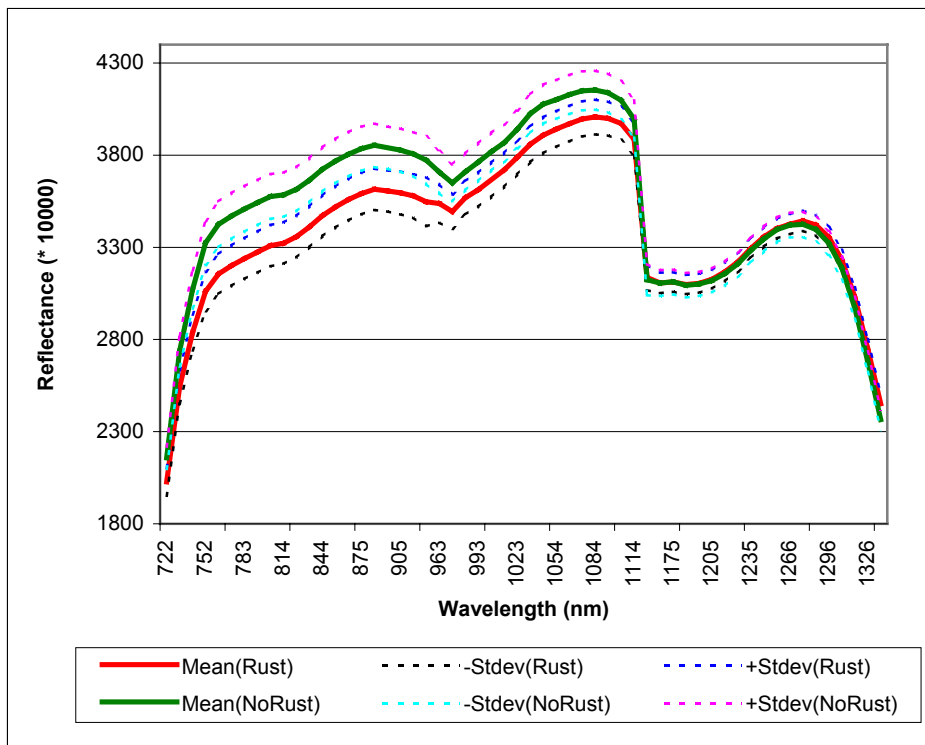


Figure 6 Mean reflectance spectra (721–1336nm) of Hyperion sample pixels containing sugarcane orange rust disease and without orange rust disease

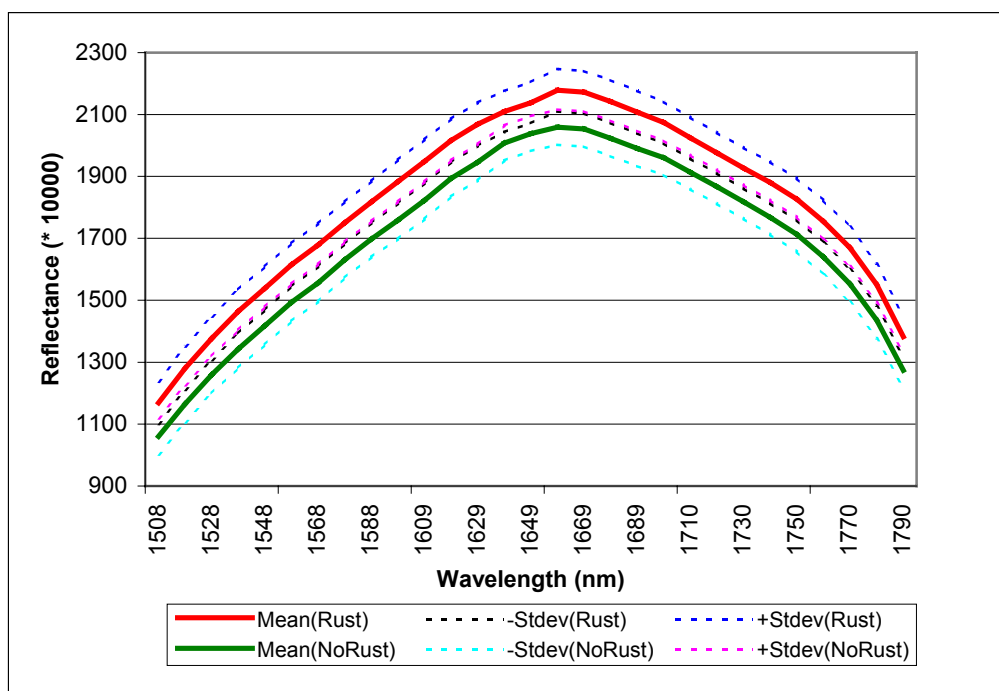


Figure 7 Mean reflectance spectra (1500–1800nm) of Hyperion sample pixels containing sugarcane orange rust disease and without orange rust disease

As anticipated, the red (680nm) and NIR (800nm) bands exhibited inverse relationship. However, spectral plots showed that there are other bands (i.e. those that can be paired with NIR) with inverse relationship with NIR, but have greater difference in magnitude than red band:

- green band (550nm) (figure 5)
- SWIR band (1660nm) (figure).

Thus, in theory, it may be better for band ratioing to use green-NIR or SWIR-NIR band combinations, rather than the red-NIR bands.

The results of the discriminant function analysis (tables 2 and 3) confirmed that this is the case. The 1600nm (SWIR) band, if combined (by ratioing) with either NIR band (800nm) or green band (550nm), will produce the best (highest correlation and classification accuracy) among the indices. The indices include *DWSI-1*, *DSWI-2*, *DSWI-5* and *MSI*. The top three indices were formulated using the procedures employed in this study.

The discriminant function attained a classification accuracy of 96.9% for the unselected ‘hold out’ sample (Table 4). This result is considered very high, and can be attributed to the following reasons:

- there is inherent high spectral separability between healthy sugarcane crops and diseased crops at moderate to advanced stage
- the Hyperion sensor’s ability to capture images at contiguous narrow bands enabled spectral differences to become more statistically separable
- the number of categories used in the classification is minimum, i.e. only two classes.

In a forest classification study in Canada, Hyperion obtained 92.9% classification accuracy while Landsat ETM+ has 75.0% (Goodenough, et al., 2002).

Table 2 Structure matrix from the discriminant function^c

Index ^a	Correlation ^b	Index ^a	Correlation ^b
1. DWSI-1	-.839	21. ND750/705	-.439
2. DWSI-2	.835	22. SR750/705	-.433
3. DWSI-5	-.811	23. MCARI	-.405
4. MSI	.803	24. SR695/420	.404
5. NDWI_Hyp	-.796	25. PSSRb	-.403
6. NDWI	-.749	26. WW983	-.361
7. Ave (750 to 850)	-.703	27. WW1205/PSSRa	-.358
8. SIPI	.629	28. TCARI/OSAVI	-.326
9. WW1205	-.627	29. WI/ND750/660	.309
10. PC1	.610	30. SR750/550	-.282
11. PC2	-.603	31. PSRI	.229
12. DWSI-4	-.563	32. SR800/550	-.227
13. ND800/680	-.508	33. DSWI-3	.166
14. SR695/760	.507	34. WI	-.150
15. OSAVI	-.496	35. Green-well	.126
16. TCARI	-.493	36. PRI	.094
17. PSSRa	-.493	37. REIP-Lagr	-.079
18. ND750/660	-.490	38. Chloro-well	-.077
19. MND750/705	-.477	39. WW983/PSSRa	.077
20. MSR705/445	-.474	40. REIP-poly	-.029

^a Variables ordered by absolute size of correlation within function.

^b Pooled within-groups correlations between discriminating variables and standardised canonical discriminant function.

^c The discriminant function (linear combination of DSWI-2, SR695/420, and NDWI-Hyp) results to 96.9% classification accuracy.

Table 3 Canonical correlation and classification accuracy for the single-variable run (predictor variable entered one at a time)

Index ^a	Correlation ^b & Accuracy ^c	Index ^a	Correlation ^b & Accuracy ^c
1. DWSI-2	.785 (92.9%)	21. ND750/705	.578 (75.5%)
2. DWSI-1	.781 (94.9%)	22. SR750/705	.569 (75.5%)
3. DWSI-5	.781 (93.9%)	23. MCARI	.534 (77.6%)
4. NDWI	.780 (93.9%)	24. SR695/420	.523 (83.7%)
5. NDWI_Hyp	.770 (94.9%)	25. PSSRb	.518 (73.5%)
6. MSI	.765 (92.9%)	26. WW983	.493 (72.6%)
7. Ave (750 to 850)	.739 (87.8%)	27. TCARI/OSAVI	.459 (69.4%)
8. DWSI-4	.709 (88.8%)	28. WW1205/PSSRa	.379 (66.3%)
9. SIPI	.698 (85.7%)	29. WI/ND750/660	.355 (66.3%)
10. WW1205	.649 (84.7%)	30. PSRI	.364 (65.3%)
11. PC2	.635 (82.7%)	31. WI	.350 (70.4%)
12. ND800/680	.632 (86.7%)	32. SR750/550	.296 (65.3%)
13. PSSRa	.632 (85.7%)	33. SR800/550	.238 (64.3%)
14. SR695/760	.630 (84.7%)	34. WW983/PSSRa	.234 (56.1%)
15. PC1	.623 (90.8%)	35. DSWI-3	.121 (62.2%)
16. TCARI	.620 (79.6%)	36. Green-well	.116 (52.0%)
17. OSAVI	.617 (85.7%)	37. REIP-Lagr	.112 (59.2%)
18. ND750/660	.605 (83.7%)	38. PRI	.041 (65.3%)
19. MND750/705	.603 (79.6%)	39. Chloro-well	.025 (56.1%)
20. MSR705	.590 (76.5%)	40. REIP-Poly	.004 (48.0%)

^a Variables ordered by size of correlation.

^b Interpretation is equivalent to Pearson correlation coefficient.

^c Accuracy is based from unselected ('hold-out sample') original grouped cases

Table 4 Classification results for discriminant function analysis (stepwise variable selection method)^{b,c,d}

				Predicted Group Membership		Total
				0	1	
Cases Selected	Original	Count	0	105	6	111
			1	11	81	92
		%	0	94.6	5.4	100.0
	Cross-validated ^a	Count	0	105	6	111
			1	11	81	92
		%	0	94.6	5.4	100.0
Cases Not Selected	Original	Count	0	47	1	48
			1	2	48	50
		%	0	97.9	2.1	100.0
	Cross-validated ^a	Count	0	47	1	48
			1	2	48	50
		%	0	97.9	2.1	100.0

^a Cross validation is done only for those cases in the analysis. In cross validation, each case is classified by the functions derived from all cases other than that case.

^b 91.6% of selected original grouped cases correctly classified.

^c 96.9% of unselected original grouped cases correctly classified.

^d 91.6% of selected cross-validated grouped cases correctly classified.

This study shows that spectral discrimination of sugarcane orange rust disease (with moderate to high severity of infection) can be significantly improved by incorporating selected band in the SWIR region. The indices that only used selected bands in the VNIR (e.g. *Ave(750 to 850)*, *SIPi*, *DSWI-4*, *ND800/600*, *OSAVI*, *TCARI*, *PSSRa*, etc.) performed moderately. The indices developed from the reflectance red-edge (690–720nm) (e.g. *REIP-Lagr* and *REIP-poly*) performed very poorly in discriminating diseased from non-diseased sugarcane crops.

Conclusions

The empirical-statistical approach we used in this study allowed us to systematically formulate and assess new and existing vegetation indices for sugarcane disease detection. Interactive visual interpretation of spectral plots, focusing on the magnitude of difference and the direction of relationship of sample pixel values, allowed the identification of candidate bands for index formulation. The discriminant function analysis facilitated the assessment of each index (and its relative utility) based on their correlations with the output model and classification accuracy statistics. The incorporation of 1660nm SWIR band led to the formulation of several variations of 'Disease-Water Stress Indices' (DSWI) that yielded better discrimination of sugarcane orange rust disease. While these new indices were based from local and empirical evidences, and hence may lack portability, they are still important in generating cumulative knowledge for SVI development. They need to be tested for other crops and/or different local areas, including the implications of crop growth stages and the severity levels of infection.

Acknowledgments

We thank Guy Byrne and Alan Marks (CSIRO) for their help during the field work. The mathematical formulation of *DSWI-5* index was suggested by Peter Dunn (USQ). Bisun Datt (CSIRO) provided valuable advice during the pre-processing of Hyperion imagery.

References

- Analytical Imaging and Geophysics LLC 2002. *ACORN Version 4.10*. AIG, Boulder.
- Apan, A. and Held, A. 2002. *In-House Workshop On Hyperion Data Processing: Echo-ing The Sugarcane Project Experience*. CSIRO Land and Water, Black Mountain Laboratories, Canberra.
- Apan, A., Held, A., Phinn, S. and Markley, J. *submitted*. Detecting Sugarcane 'Orange Rust' Disease Using EO-1 Hyperion Hyperspectral Imagery. *International Journal of Remote Sensing*.
- Bannari, A., Asalhi, H. and Teillet, P.M. 2002. Transformed Difference Vegetation Index (TDVI) for Vegetation Cover Mapping, *Proceedings of the 2002 IEEE IGARSS and 24th Canadian Symposium on Remote Sensing, Toronto, Canada, 24–28 June 2002*, np.
- Barry, P. 2001. *EO-1/ Hyperion Science Data User's Guide, Level 1_B*. TRW Space, Defence and Information Systems, Redondo Beach, CA.
- Blackburn, G.A. 1998. Spectral indices for estimating photosynthetic pigment concentrations: a test using senescent tree leaves. *International Journal of Remote Sensing*, 19, 657–675.
- Boardman, J.W. 1998. Post-ATREM Polishing of AVIRIS apparent reflectance data using EFFORT: a lesson in accuracy versus precision. *Summaries of the Seventh JPL Airborne Earth Science Workshop 12–16 January 1998*, p.53, JPL, Pasadena.
- Broge, N.H. and LeBlanc, E. 2001. Comparing prediction power and stability of broadband and hyperspectral vegetation indices for estimation of green leaf area index and canopy chlorophyll density. *Remote Sensing of the Environment*, 76, 156–172.
- Carter, G.A. 1994. Ratios of leaf reflectances in narrow wavebands as indicators of plant stress, *International Journal of Remote Sensing*, 15, 697–703.
- Croft, B., Magarey, R. and Whittle, P. 2000. Disease Management. In *Manual of Canegrowing*, edited by M. Hogarth and P. Allsopp. pp. 263–289, Bureau of Sugar Experiment Stations, Brisbane.
- Datt, B., McVicar, T.R., Van Niel, T.G., Jupp, D.L.B. and Pearlman, J. S. (submitted). Pre-processing EO-1 Hyperion hyperspectral data to support the application of agricultural indices, *IEEE Transactions on Geoscience and Remote Sensing*.
- Daughtry, C.S.T., Gallo, K.P., Goward, S.N., Prince, S.D. and Kustas, W.P. 1992. Spectral estimates of absorbed radiation and phytomass production in corn and soybean canopies. *Remote Sensing of Environment* **39**, 141–152.
- Daughtry, C.S.T., Walthall, C.L., Kim, M.S., Brown De Colstoun, E., and McMurtrey III, J.E. 2000. Estimating corn leaf chlorophyll concentration from leaf and canopy reflectance. *Remote Sensing of Environment*, 74, 229–239.
- Dawson, T.P. and Curran, P.J. 1998. A new technique for interpolating the reflectance red edge position. *International Journal of Remote Sensing*, 19, 2133–2139.
- Gamon, J.A., Peñuelas, J. and Field, C.B. 1992. A narrow-waveband spectral index that tracks diurnal changes in photosynthetic efficiency. *Remote Sensing of Environment*, 41, 35–44.
- Gao, B., 1996. NDWI—A Normalized Difference Water Index for Remote Sensing of Vegetation Liquid Water from Space. *Remote Sensing of Environment*, 58, 257–266.
- Gitelson, A.A. and Merzlyak, M.N., 1994. Spectral reflectance changes associate with autumn senescence of *Aesculus hippocastanum* L. and *Acer platanoides* L. leaves. Spectral features and relation to chlorophyll estimation. *Journal of Plant Physiology*, 143, 286–292.

- Govaert, Y.M., Verstraete, M.M., Pinty, B., and Gobron, N., et al. 1999. Designing optimal spectral indices: a feasibility and proof of concept study, *International Journal of Remote Sensing*, 20(9), 1853–1873.
- Haboudane, D, Miller, J.R., Tremblay, N., Zarco-Tejada, P.J., and Dextraze, L. 2002. Integrated narrow-band vegetation indices for prediction of crop chlorophyll content for application to precision agriculture. *Remote Sensing of Environment*, 81, 416–426.
- Huete, A. R. 1988. A soil-adjusted vegetation index (SAVI). *Remote Sensing of Environment*, 25, 295–309.
- Hunt, E.R. and Rock, B.N. 1989. Detection of changes in leaf water content using near- and middle-infrared reflectances. *Remote Sensing of Environment*, 30, 43–54.
- Kaufman, Y.J. and Tanre, D. 1992. Atmospherically Resistant Vegetation Index (ARVI) for EOS-MODIS, *IEEE Transactions on Geoscience and Remote Sensing*, 30(2), 261–270.
- Kumar, L., Schmidt, K.S., Dury, S., and Skidmore, A. 2001. Imaging Spectrometry and Vegetation Science. In *Imaging Spectrometry, Basic Principles and Prospective Applications*, edited by F.D. van der Meer and S.M. de Jong, pp. 111–155, Kluwer Academic Publishers, Dordrecht.
- Merzlyak, M.N., Gitelson, A.A., Chivkunova, O.B. and Rakitin, V.Y. 1999. Non-destructive optical detection of pigment changes during leaf senescence and fruit ripening. *Physiologica Plantarum*, 106, 135–141.
- Pearlman, J., Carman, S., Segal, C., Jarecke, P. and Barry, P. 2001. Overview of the Hyperion Imaging Spectrometer for the NASA EO-1 Mission, *Proceedings of the International Geoscience and Remote Sensing Symposium (IGARSS '01)*, Sydney, Australia, July 9–13, 2001.
- Peñuelas, J., Baret, F., and Filella, 1995. Semi-empirical indices to assess carotenoids/chlorophyll a ratio from leaf spectral reflectance. *Photosynthetica*, 31, 221–230.
- Peñuelas, J., Pinol, R.O. Ogaya, R., and Filella, 1997. Estimation of plant water concentration by the reflectance Water Index WI (R900/R970), *International Journal of Remote Sensing*, 18, 2869–2875.
- Rondeaux, G., Steven, M., and Baret, F. 1996. Optimization of Soil-Adjusted Vegetation Indices. *Remote Sensing of Environment*, 55, 95–107.
- Rouse, J.W., Haas, R.H., Schell, J.A., and Deering, D.W. 1973. Monitoring Vegetation Systems in the Great Plains with ERTS, *Proceedings of the Third Earth Resources Technology Satellite-1 Symposium*, Greenbelt, NASA SP-351, vol. 1, pp. 309–317, U.S. Government Printing Office, Washington, D.C.
- Sims, D.A. and Gamon, J.A., 2002, Relationship between leaf pigment content and spectral reflectance across a wide range of species, leaf structures and developmental stages. *Remote Sensing of Environment*, 81, 337–354.
- SPSS 2001. *SPSS for Windows* (Release 11). SPSS, Chicago.
- Strachan, I. B., Pattey, E., and Boisvert, J.B. 2002. Impact of nitrogen and environmental conditions on corn as detected by hyperspectral reflectance. *Remote Sensing of Environment*, 80, 213–224.
- Tucker, C.J. 1979. Red and photographic infrared linear combinations for monitoring vegetation. *Remote Sensing of Environment*, 8, 127–150.
- Tucker, C.J., Vanpraet, C.L., Sharman, M.J. and van Ittersum, G. 1985. Satellite remote sensing of total herbaceous biomass production in the Senegalese Sahel: 1980–1984. *Remote Sensing of Environment*, 17:233–249.
- Ustin, S.L., Roberts, D.A. Gardner, M. and Dennison, P. 2002. Evaluation of the Potential of Hyperion Data to Estimate Wildfire Hazard in the Santa Ynez Front Range, Santa Barbara, California. *Proceedings of the 2002 IEEE IGARSS and 24th Canadian Symposium on Remote Sensing, Toronto, Canada, 24–28 June 2002*, pp. 796–798.